JACS
JOURNAL OF THE AMERICAN CHEMICAL SOCIETY
pubs.acs.org/JACS
Communication

An Atomistic Picture of Boron Oxide Catalysts for Oxidative Dehydrogenation Revealed by Ultrahigh Field $^{11}B-^{17}O$ Solid-State NMR Spectroscopy

Rick W. Dorn, Lesli O. Mark, Ivan Hung, Melissa C. Cendejas, Yijue Xu, Peter L. Gor'kov, Wenping Mao, Faysal Ibrahim, Zhehong Gan,* Ive Hermans,* and Aaron J. Rossini*

Cite This: J. Am. Chem. Soc. 2022, 144, 18766−18771
Read Online
ACCESS | Metrics & More | Article Recommendations | Supporting Information

ABSTRACT: Boron oxide/hydroxide supported on oxidized activated carbon (B/OAC) was shown to be an inexpensive catalyst for the oxidative dehydrogenation (ODH) of propane that offers activity and selectivity comparable to boron nitride. Here, we obtain an atomistic picture of the boron oxide/hydroxide layer in B/OAC by using 35.2 T ^{11}B and ^{17}O solid-state NMR experiments. NMR spectra measured at 35.2 T resolve the boron and oxygen sites due to narrowing of the central-transition powder patterns. A 35.2 T 2D $^{11}B\{^{17}O\}$ dipolar heteronuclear correlation NMR spectrum revealed the structural connectivity between boron and oxygen atoms. The approach outlined here should be generally applicable to determine atomistic structures of heterogeneous catalysts containing quadrupolar nuclei.

Boron-based heterogeneous catalysts, such as hexagonal boron nitride (*h*-BN) and silica or carbon-supported boron oxides, are highly selective catalysts for the oxidative dehydrogenation (ODH) of propane to propylene and exhibit minimal overoxidation to undesirable CO_x products.[1−12] Comprehensive structural characterization of boron-based ODH catalysts, primarily by solid-state NMR spectroscopy, has revealed that clusters of boron oxide/hydroxide $[\mathbf{B}(OB)_x(OH)_{3-x}]$ are the catalytically active sites.[5,13−15] For example, with ultrahigh field 35.2 T ^{11}B solid-state NMR spectroscopy, we showed that the ODH active boron oxide/hydroxide layer grows directly off the *h*-BN framework under reactions conditions, explaining why induction periods of >4 h are required before optimal catalytic performance is reached.[15]

The understanding that large networks of clustered boron oxide/hydroxide are the ODH active sites enabled rational design and development of an oxidized activated carbon supported boron catalyst (B/OAC) that contains high boron loadings (∼28 wt % B).[8] B/OAC exhibits near identical propylene selectivity as the benchmark *h*-BN catalyst, but is twice as active per mass of catalyst and less expensive to make.[8]

Low-field solid-state NMR spectroscopy, in conjunction with infrared, Raman, and X-ray photoelectron spectroscopies, revealed that at least 80% of boron is clustered on the support.[8] However, a complete picture of the boron layer in B/OAC ODH catalysts is lacking. In particular, ^{11}B solid-state NMR spectroscopy alone only provides information on the extent of boron oxide/hydroxide clustering and not on the specific oxide species, i.e., linear-type borates, ring-type borates, and relative populations of bridging B-**O**-B species to B-**O**-H hydroxyl groups.[15] Here, we use 35.2 and 18.8 T ^{11}B and ^{17}O solid-state NMR spectroscopy to obtain a complete atomistic picture of B/OAC.

B/OAC was ^{17}O enriched via impregnation of the synthesized catalyst with 40% $^{17}OH_2$ (see Methods in Supporting Information). The final ^{17}O-enrichment level is estimated to be ca. 18% (vide infra). One-dimensional (1D) ^{11}B NMR spectra were recorded at B_0 = 14.1, 18.8, or 35.2 T (Figure 1A). The solid-state NMR spectra of half-integer quadrupolar nuclei such as ^{11}B and ^{17}O show improved resolution at 35.2 T due to a decrease in the second-order quadrupolar broadening of the central-transition (CT). The resolution approximately increases with the square of B_0. The advantages of 35.2 T solid-state NMR spectroscopy[16] of half-integer quadrupolar nuclei for materials science applications have been demonstrated.[15,17−25]

The 35.2 T ^{11}B NMR spectrum reveals three-coordinate BO_3 NMR signals with isotropic chemical shifts (δ_{iso}) of ca. 19.6, 18.5, 16.6, 14.1, 11.2, and 8.0 ppm (Figure 1A and Table S1). There are additional weak ^{11}B NMR signals near 0 ppm assigned to BO_4 sites. The low-frequency ^{11}B sites exhibit increased relative signal intensity with the use of a 0.5 s recycle delay (Figure S1). We note that the lower-frequency ^{11}B NMR signals are not unique and display large chemical shift distributions, typical of disordered and amorphous materials.

35.2 T 2D $^{11}B\{^{1}H\}$ dipolar heteronuclear multiple quantum correlation (D-HMQC) NMR spectra primarily shows high-frequency ^{11}B NMR signals ($\delta_{iso} \geq$ ca. 16 ppm), suggesting these correspond to B-OH groups; however, the lower

Received: August 3, 2022
Published: October 10, 2022

https://doi.org/10.1021/jacs.2c08237
J. Am. Chem. Soc. 2022, 144, 18766−18771

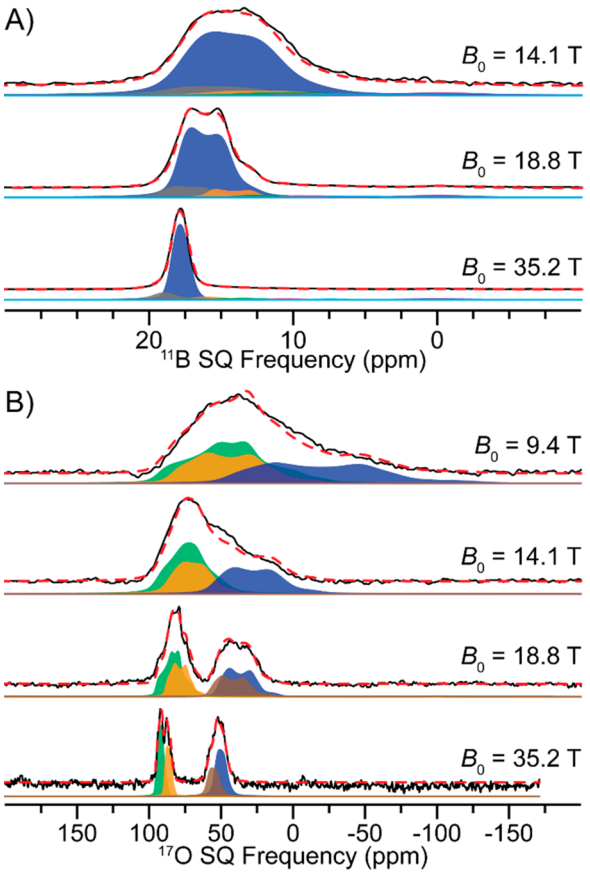

Figure 1. 1D (A) ^{11}B and (B) ^{17}O MAS solid-state NMR spectra of B/OAC. The (black) solid and (red) dashed lines correspond to the experimental and analytically simulated NMR spectra, respectively.

frequency ^{11}B sites also appear spatially proximate to −OH species (Figure S2). In addition, a 35.2 T 2D ^{11}B double-quantum-single-quantum (DQ-SQ)[26,27] homonuclear correlation NMR spectrum illustrates that all boron is clustered (i.e., exhibiting B-O-B bonds; Figure S3). Therefore, the high-frequency ^{11}B NMR signals correspond to $\mathbf{B}(OB)_x(OH)_{3-x}$ (x = 1−3) sites.[15,25,28−32] The assignment of the ^{11}B NMR signals to specific $\mathbf{B}(OB)_x(OH)_{3-x}$ (x = 1−3) species is challenging because the chemical shift may change by a few ppm depending on the number of **B**-OH/**B**-OB bonds and the specific oxide structure (i.e., ring versus linear borate). However, the 2D ^{11}B{^{1}H}, ^{17}O{^{1}H} and ^{11}B{^{17}O} heteronuclear correlation experiments confirm the assignment of the primary boron NMR signals to $\mathbf{B}(OB)_x(OH)_{3-x}$ species. The lower-frequency ^{11}B NMR signals exhibit attenuated signal intensity in the 2D ^{11}B DQ-SQ NMR spectrum as compared to the 1D ^{11}B NMR spectrum, consistent with our previous assignment to boron grafted to carbon (i.e., B-O-C bonds).[8] Simulation of the 35.2 T ^{11}B NMR spectrum reveals that $\mathbf{B}(OB)_x(OH)_{3-x}$ sites (δ_{iso}(^{11}B) ≥ ca. 16 ppm) correspond to ca. 95% of boron, while only ca. 5% correspond to carbon grafted species (δ_{iso}(^{11}B) ≤ ca. 14 ppm; Figure 1A and Table S1).

1D ^{17}O NMR spectra were recorded at B_0 = 9.4, 14.1, 18.8, or 35.2 T (Figure 1B). At 9.4 or 14.1 T, all ^{17}O NMR signals are overlapping, while at B_0 = 18.8 or 35.2 T, ^{17}O NMR signals centered at ca. 50 and 90 ppm are clearly resolved and are assigned to hydroxyl groups (B-**O**H) and bridging oxygen atoms (B-**O**-B), respectively. The 35.2 T NMR spectrum reveals two distinct bridging oxygen ^{17}O NMR signals (Figure 1B and S4). A 2D ^{17}O multiple-quantum magic-angle spinning (MQMAS)[33−35] NMR spectrum recorded at B_0 = 18.8 T clearly shows two unique B-**O**-B ^{17}O NMR signals as were observed in the 1D 35.2 T ^{17}O NMR spectrum (Figure 2A).

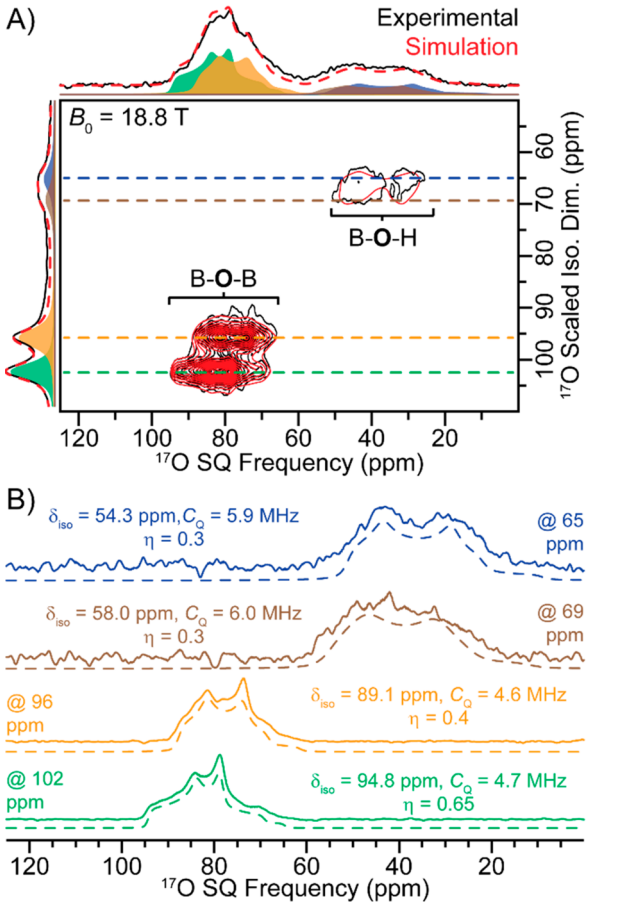

Figure 2. (A) 2D ^{17}O MQMAS NMR spectrum of B/OAC. The black and red lines correspond to the experimental and analytically simulated NMR spectra, respectively. (B) ^{17}O MAS NMR spectra extracted from the isotropic dimension of the 2D MQMAS at the indicated shifts.

Notably, the 1D 35.2 T ^{17}O NMR spectrum has only slightly lower resolution than the ^{17}O isotropic MQMAS dimension but was acquired 40 times faster and is quantitative. The B-**O**-H ^{17}O NMR signals exhibit a δ_{iso} between 54 and 60 ppm, C_Q ∼ 6 MHz and η = 0.3 (Figure 2B). The distribution in δ_{iso}(^{17}O) likely results from differences in local hydrogen bonding interactions. Interestingly, the two B-**O**-B ^{17}O NMR signals exhibit significantly different η values of 0.4 (δ_{iso} = 89.1 ppm) or 0.65 (δ_{iso} = 94.8 ppm), while C_Q is ca. 4.6 MHz (Figure 2B). Dupree and co-workers observed a similar set of B-**O**-B ^{17}O NMR signals in vitreous B_2O_3 via ^{17}O MQMAS and DOuble-Rotation (DOR) NMR spectroscopy.[36] With the aid of quantum chemical calculations, they showed that the low (0.4) and high (0.7) η ^{17}O NMR signals correspond to linear and ring-type B-**O**-B units, respectively. The boron oxide/hydroxide phase of B/OAC clearly contains both linear and ring-type B-**O**-B species, consistent with a prior Raman spectroscopy study.[8]

2D ^{17}O{^{1}H} D-HMQC NMR spectra were recorded at B_0 = 18.8 T with either a short (0.25 ms) or long (1.5 ms) duration

https://doi.org/10.1021/jacs.2c08237
J. Am. Chem. Soc. 2022, 144, 18766−18771

of $SR4_1^2$ dipolar recoupling.[37] The 2D $^{17}O\{^1H\}$ D-HMQC NMR spectrum recorded with a short duration of dipolar recoupling shows only the low-frequency ^{17}O NMR signals, confirming their assignment to B-**O**-H hydroxyl groups (Figure 3, blue). At longer durations of dipolar recoupling, all ^{17}O NMR signals are observed (Figure 3, red). Importantly, the ^{17}O projection from the D-HMQC spectrum recorded with 1.5 ms of recoupling resembles the direct excitation ^{17}O NMR spectrum, implying that the hydroxyl groups are homogeneously distributed throughout the boron layer.

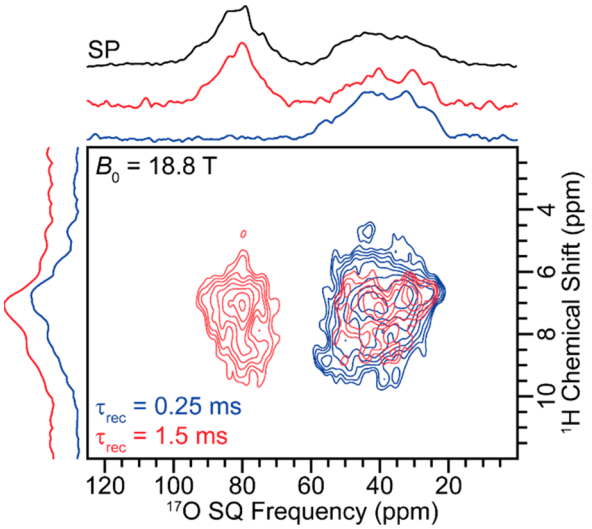

Figure 3. 2D $^{17}O\{^1H\}$ D-HMQC NMR spectra of B/OAC recorded with either (blue) 0.25 or (red) 1.5 ms of total $SR4_1^2$ heteronuclear dipolar recoupling applied to the ^1H spins. A quantitative, single-pulse (SP) ^{17}O NMR spectrum is shown for comparison.

$^{17}O\{^{11}B\}$ *J*-Resolved experiments with CT-selective ^{11}B inversions pulses were performed to unambiguously confirm the assignment of all ^{17}O NMR signals (Figure S5). The extent of signal dephasing in a *J*-Resolved experiment is dependent on the number of boron atoms covalently bonded to oxygen, the ^{11}B isotopic abundance and percent of ^{11}B spins residing in the CT spin states (see Supporting Information for more discussion). Analytical simulations that take into account the statistical probability of having an attached ^{11}B spin in the CT spin state reveal that the high- and low-frequency sets of ^{17}O NMR signals have either two or one covalently bonded boron atom, respectively, directly confirming their assignments to B-**O**-B and B-**O**-H. The ^{17}O-enrichment level was estimated to be ca. 18% by analytically simulating an $^{11}B\{^{17}O\}$ *J*-Resolved curve recorded with a CT-selective ^{17}O inversion pulse (Figure S6, see Supporting Information for more discussion).[38]

With complete ^{17}O NMR signal assignment on hand, the population of all ^{17}O species was determined by analytically simulating the 35.2 T 1D ^{17}O NMR spectrum (Figures 1B and S4, Table S2). Interestingly, there is a ca. 1:1 ratio of bridging oxygen atoms (B-**O**-B) to hydroxyl groups (B-**O**-H), revealing that the boron oxide/hydroxide layer is very hydroxyl dense. The amount of hydroxyl groups may decrease under reaction conditions due to the high temperatures used for catalysis (ca. 550 °C); however, the room-temperature NMR experiments still provide valuable insight into the ambient structure of highly active ODH catalysts. The 35.2 T magnetic field provided resolution between the ring and linear-type borate bridging O atoms, enabling their populations to be accurately determined (Figure S4). There is a ca. 4:3 ratio of ring to linear-type borate species, illustrating that many of the B/O atoms are present within a ring (Table S2). We note that the relatively high level of ^{17}O-enrichment, the high proportion of -OH groups indicated in both the ^{17}O NMR experiments and $^{11}B\{^1H\}$ D-HMQC experiments (Figure S2), and the similarity of the 1D ^{11}B spin echo spectra and the ^{11}B projection NMR spectrum from the 2D $^{11}B\{^{17}O\}$ D-HMQC spectrum (Figure 4) all suggest that the ^{17}O enrichment was uniform and that the ^{17}O NMR spectra are indeed quantitative.

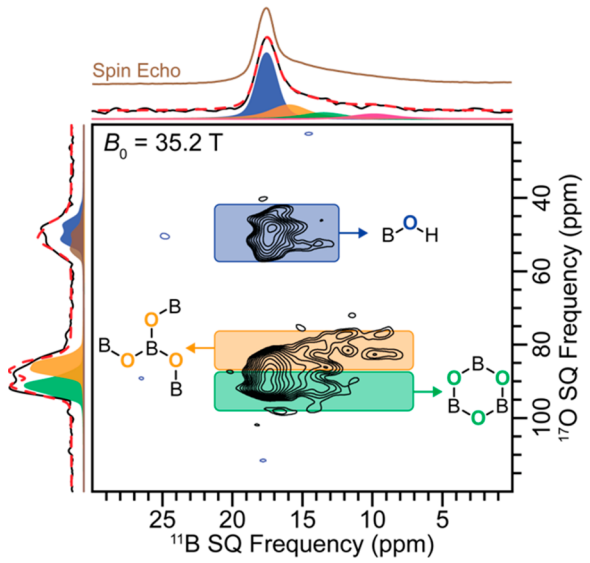

Figure 4. 2D $^{11}B\{^{17}O\}$ D-HMQC NMR spectrum of B/OAC recorded at B_0 = 35.2 T with 0.8 ms of REDOR recoupling applied to the ^{11}B spins.

Lastly, we recorded 2D $^{11}B\{^{17}O\}$ D-HMQC NMR spectra at B_0 = 14.1 T, 18.8 or 35.2 T (Figures 4 and S7–S8). We note that several groups have developed techniques for challenging 2D correlation NMR experiments involving half-integer quadrupolar nuclei.[38−41] The $^{11}B\{^{17}O\}$ D-HMQC NMR spectrum greatly benefits from acquisition at ultrahigh field due to significant CT line narrowing in both dimensions. With a B_0 of 18.8 T or 35.2 T, the B-**O**-B and B-**O**-H ^{17}O NMR signals are clearly resolved in the 2D HMQC spectra. However, with a B_0 of 35.2 T, unique correlations between ^{11}B and the linear or ring-type borate ^{17}O NMR signals are distinguishable. In addition to the dramatic increase in resolution, there are also large sensitivity gains. The 2D $^{11}B\{^{17}O\}$ D-HMQC NMR spectra acquired at B_0 = 14.1 T, 18.8 or 35.2 T were recorded in ca. 38, 15, or 3 h, respectively.

The 35.2 T $^{11}B\{^{17}O\}$ D-HMQC NMR spectrum shows that the high frequency ^{11}B NMR signals correlate with all ^{17}O NMR signals, consistent with the high population of these ^{11}B sites and suggesting a homogeneous distribution of hydroxyl groups and linear and ring-type borate species. Interestingly, the low-frequency ^{11}B NMR signals predominantly correlate with the linear-type bridging oxygen atoms, suggesting that the boron oxide/hydroxide layer is grafted to the carbon surface via linear-type borate groups.

In conclusion, ultrahigh field 35.2 T ^{11}B and ^{17}O solid-state NMR spectroscopy enabled us to reveal a complete atomistic picture of the boron oxide and hydroxide layer in B/OAC

https://doi.org/10.1021/jacs.2c08237
J. Am. Chem. Soc. 2022, 144, 18766−18771

ODH catalysts (Figure 5). The simplified structural model shown in Figure 5 is not necessarily unique but represents the

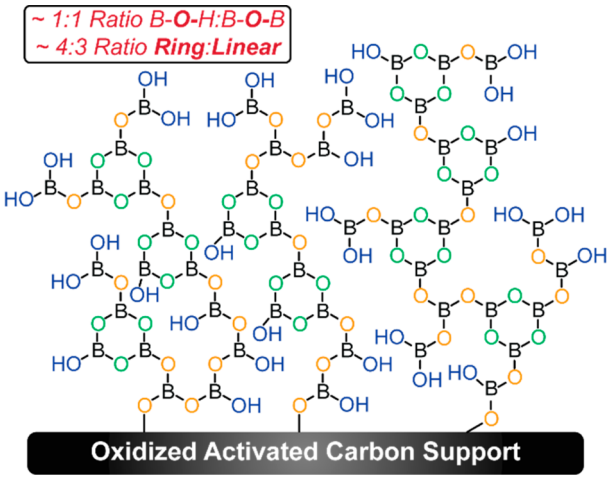

Figure 5. Structural model of the boron oxide/hydroxide layer grafted to the OAC support. The color of O atoms correspond to the ^{17}O NMR analytical fits.

type of species found within the boron layer. Over 90% of boron is clustered and located within the amorphous oxidized/hydrolyzed layer, while only a small fraction of boron is grafted on the carbon support. Hydroxyl groups (B-**O**-H) are homogeneously distributed throughout the active phase and are highly abundant (ca. 1:1 ratio B-**O**-H: B-**O**-B), suggesting that a majority of boron takes the form $\mathbf{B}(OB)_2(OH)$ or $\mathbf{B}(OB)(OH)_2$. There is a ca. 4:3 ratio of ring to linear-type bridging oxygen atoms. Based on the populations of all oxygen species, a majority of hydroxyl groups likely terminate linear-borate species [i.e., $\mathbf{B}(OB)(OH)_2$]. The 35.2 T 2D $^{11}B\{^{17}O\}$ D-HMQC NMR spectrum suggests a relatively homogeneous distribution of linear and ring-type borate groups. These findings suggest that any type of boron oxide clusters on a support should be active for ODH of light olefins. However, a careful assessment of how the relative population of hydroxyl groups and ratio of linear to ring-type borate species affect ODH performance should be explored. We anticipate that ultrahigh field NMR spectroscopy will become more routine in revealing atomistic structural models of active sites within heterogeneous catalysts containing quadrupolar nuclei.

■ ASSOCIATED CONTENT

Data Availability Statement

Raw NMR spectroscopy data is available for download at DOI: 10.5281/zenodo.6954698.

Supporting Information

The Supporting Information is available free of charge at https://pubs.acs.org/doi/10.1021/jacs.2c08237.

Synthetic and solid-state NMR methods, additional solid-state NMR spectra, and solid-state NMR experimental parameters (PDF)

■ AUTHOR INFORMATION

Corresponding Authors

Zhehong Gan − *National High Magnetic Field Laboratory (NHMFL), Tallahassee, Florida 32310, United States;* orcid.org/0000-0002-9855-5113; Email: gan@magnet.fsu.edu

Ive Hermans − *University of Wisconsin − Madison, Department of Chemistry, Madison, Wisconsin 53706, United States; University of Wisconsin − Madison, Department of Chemical and Biological Engineering, Madison, Wisconsin 53706, United States;* orcid.org/0000-0001-6228-9928; Email: hermans@chem.wisc.edu

Aaron J. Rossini − *Department of Chemistry, Iowa State University, Ames, Iowa 50011, United States; U.S. Department of Energy, Ames National Laboratory, Ames, Iowa 50011, United States;* orcid.org/0000-0002-1679-9203; Email: arossini@iastate.edu

Authors

Rick W. Dorn − *Department of Chemistry, Iowa State University, Ames, Iowa 50011, United States; U.S. Department of Energy, Ames National Laboratory, Ames, Iowa 50011, United States*

Lesli O. Mark − *University of Wisconsin − Madison, Department of Chemistry, Madison, Wisconsin 53706, United States;* orcid.org/0000-0003-1746-7638

Ivan Hung − *National High Magnetic Field Laboratory (NHMFL), Tallahassee, Florida 32310, United States;* orcid.org/0000-0001-8916-739X

Melissa C. Cendejas − *University of Wisconsin − Madison, Department of Chemistry, Madison, Wisconsin 53706, United States*

Yijue Xu − *National High Magnetic Field Laboratory (NHMFL), Tallahassee, Florida 32310, United States*

Peter L. Gor'kov − *National High Magnetic Field Laboratory (NHMFL), Tallahassee, Florida 32310, United States*

Wenping Mao − *National High Magnetic Field Laboratory (NHMFL), Tallahassee, Florida 32310, United States*

Faysal Ibrahim − *University of Wisconsin − Madison, Department of Chemistry, Madison, Wisconsin 53706, United States;* orcid.org/0000-0003-3354-8104

Complete contact information is available at: https://pubs.acs.org/10.1021/jacs.2c08237

Notes

The authors declare no competing financial interest.

■ ACKNOWLEDGMENTS

This work was supported by the National Science Foundation under Grant No. CBET-1916809. A.J.R. acknowledges additional support from the Alfred P. Sloan Foundation through a Sloan research fellowship. Ultrahigh field NMR experiments were performed at the National High Magnetic Field Laboratory. The National High Magnetic Field Laboratory is supported by the National Science Foundation through NSF/DMR-1644779 and the State of Florida. The Development of the 36 T Series-Connected Hybrid magnet and NMR instrumentation was supported by NSF (DMR-1039938 and DMR-0603042) and NIH GM122698.

■ REFERENCES

(1) Grant, J. T.; Carrero, C. A.; Goeltl, F.; Venegas, J.; Mueller, P.; Burt, S. P.; Specht, S. E.; McDermott, W. P.; Chieregato, A.; Hermans, I. Selective Oxidative Dehydrogenation of Propane to Propene using Boron Nitride Catalysts. *Science* **2016**, *354* (6319), 1570.

(2) Grant, J. T.; McDermott, W. P.; Venegas, J. M.; Burt, S. P.; Micka, J.; Phivilay, S. P.; Carrero, C. A.; Hermans, I. Boron and Boron-Containing Catalysts for the Oxidative Dehydrogenation of Propane. *ChemCatChem.* **2017**, *9* (19), 3623−3626.
(3) Shi, L.; Wang, D.; Song, W.; Shao, D.; Zhang, W.-P.; Lu, A.-H. Edge-hydroxylated Boron Nitride for Oxidative Dehydrogenation of Propane to Propylene. *ChemCatChem.* **2017**, *9* (10), 1788−1793.
(4) Shi, L.; Wang, D.; Lu, A.-H. A Viewpoint on Catalytic Origin of Boron Nitride in Oxidative Dehydrogenation of Light Alkanes. *Chin. J. Catal.* **2018**, *39* (5), 908−913.
(5) Lu, W.-D.; Wang, D.; Zhao, Z.; Song, W.; Li, W.-C.; Lu, A.-H. Supported Boron Oxide Catalysts for Selective and Low-Temperature Oxidative Dehydrogenation of Propane. *ACS Catal.* **2019**, *9* (9), 8263−8270.
(6) Love, A. M.; Cendejas, M. C.; Thomas, B.; McDermott, W. P.; Uchupalanun, P.; Kruszynski, C.; Burt, S. P.; Agbi, T.; Rossini, A. J.; Hermans, I. Synthesis and Characterization of Silica-Supported Boron Oxide Catalysts for the Oxidative Dehydrogenation of Propane. *J. Phys. Chem. C* **2019**, *123* (44), 27000−27011.
(7) Belgamwar, R.; Rankin, A. G. M.; Maity, A.; Mishra, A. K.; Gómez, J. S.; Trébosc, J.; Vinod, C. P.; Lafon, O.; Polshettiwar, V. Boron Nitride and Oxide Supported on Dendritic Fibrous Nanosilica for Catalytic Oxidative Dehydrogenation of Propane. *ACS Sustainable Chem. Eng.* **2020**, *8* (43), 16124−16135.
(8) Mark, L. O.; Dorn, R. W.; McDermott, W. P.; Agbi, T. O.; Altvater, N. R.; Jansen, J.; Lebrón-Rodríguez, E. A.; Cendejas, M. C.; Rossini, A. J.; Hermans, I. Highly Selective Carbon-Supported Boron for Oxidative Dehydrogenation of Propane. *ChemCatChem.* **2021**, *13*, 3611−3618.
(9) Cendejas, M. C.; Dorn, R. W.; McDermott, W. P.; Lebrón-Rodríguez, E. A.; Mark, L. O.; Rossini, A. J.; Hermans, I. Controlled Grafting Synthesis of Silica-Supported Boron for Oxidative Dehydrogenation Catalysis. *J. Phys. Chem. C* **2021**, *125* (23), 12636−12649.
(10) Sheng, J.; Yan, B.; Lu, W.-D.; Qiu, B.; Gao, X.-Q.; Wang, D.; Lu, A.-H. Oxidative dehydrogenation of light alkanes to olefins on metal-free catalysts. *Chem. Soc. Rev.* **2021**, *50* (2), 1438−1468.
(11) Liu, Z.; Yan, B.; Meng, S.; Liu, R.; Lu, W.-D.; Sheng, J.; Yi, Y.; Lu, A.-H. Plasma Tuning Local Environment of Hexagonal Boron Nitride for Oxidative Dehydrogenation of Propane. *Angew. Chem., Int. Ed.* **2021**, *60* (36), 19691−19695.
(12) Qiu, B.; Lu, W.-D.; Gao, X.-Q.; Sheng, J.; Yan, B.; Ji, M.; Lu, A.-H. Borosilicate zeolite enriched in defect boron sites boosting the low-temperature oxidative dehydrogenation of propane. *J. Catal.* **2022**, *408*, 133−141.
(13) Love, A. M.; Thomas, B.; Specht, S. E.; Hanrahan, M. P.; Venegas, J. M.; Burt, S. P.; Grant, J. T.; Cendejas, M. C.; McDermott, W. P.; Rossini, A. J.; Hermans, I. Probing the Transformation of Boron Nitride Catalysts under Oxidative Dehydrogenation Conditions. *J. Am. Chem. Soc.* **2019**, *141* (1), 182−190.
(14) Altvater, N. R.; Dorn, R. W.; Cendejas, M. C.; McDermott, W. P.; Thomas, B.; Rossini, A. J.; Hermans, I. B-MWW Zeolite: The Case Against Single-Site Catalysis. *Angew. Chem., Int. Ed.* **2020**, *59* (16), 6546−6550.
(15) Dorn, R. W.; Cendejas, M. C.; Chen, K.; Hung, I.; Altvater, N. R.; McDermott, W. P.; Gan, Z.; Hermans, I.; Rossini, A. J. Structure Determination of Boron-Based Oxidative Dehydrogenation Heterogeneous Catalysts With Ultrahigh Field 35.2 T 11B Solid-State NMR Spectroscopy. *ACS Catal.* **2020**, *10* (23), 13852−13866.
(16) Gan, Z.; Hung, I.; Wang, X.; Paulino, J.; Wu, G.; Litvak, I. M.; Gor'kov, P. L.; Brey, W. W.; Lendi, P.; Schiano, J. L.; Bird, M. D.; Dixon, I. R.; Toth, J.; Boebinger, G. S.; Cross, T. A. NMR Spectroscopy up to 35.2T using a Series-Connected Hybrid Magnet. *J. Magn. Reson.* **2017**, *284*, 125−136.
(17) Bonhomme, C.; Wang, X.; Hung, I.; Gan, Z.; Gervais, C.; Sassoye, C.; Rimsza, J.; Du, J.; Smith, M. E.; Hanna, J. V.; Sarda, S.; Gras, P.; Combes, C.; Laurencin, D. Pushing the Limits of Sensitivity and Resolution for Natural Abundance 43Ca NMR using Ultra-High Magnetic Field (35.2 T). *Chem. Commun.* **2018**, *54* (69), 9591−9594.
(18) Madsen, R. S. K.; Qiao, A.; Sen, J.; Hung, I.; Chen, K.; Gan, Z.; Sen, S.; Yue, Y. Ultrahigh-Field 67Zn NMR Reveals Short-Range Disorder in Zeolitic Imidazolate Framework Glasses. *Science* **2020**, *367* (6485), 1473.
(19) Shen, L.; Wang, Y.; Du, J.-H.; Chen, K.; Lin, Z.; Wen, Y.; Hung, I.; Gan, Z.; Peng, L. Probing Interactions of γ-Alumina with Water via Multinuclear Solid-State NMR Spectroscopy. *ChemCatChem.* **2020**, *12* (6), 1569−1574.
(20) Chen, K.; Horstmeier, S.; Nguyen, V. T.; Wang, B.; Crossley, S. P.; Pham, T.; Gan, Z.; Hung, I.; White, J. L. Structure and Catalytic Characterization of a Second Framework Al(IV) Site in Zeolite Catalysts Revealed by NMR at 35.2 T. *J. Am. Chem. Soc.* **2020**, *142* (16), 7514−7523.
(21) Chen, C.-H.; Gaillard, E.; Mentink-Vigier, F.; Chen, K.; Gan, Z.; Gaveau, P.; Rebière, B.; Berthelot, R.; Florian, P.; Bonhomme, C.; Smith, M. E.; Métro, T.-X.; Alonso, B.; Laurencin, D. Direct 17O Isotopic Labeling of Oxides Using Mechanochemistry. *Inorg. Chem.* **2020**, *59* (18), 13050−13066.
(22) Wang, Q.; Li, W.; Hung, I.; Mentink-Vigier, F.; Wang, X.; Qi, G.; Wang, X.; Gan, Z.; Xu, J.; Deng, F. Mapping the Oxygen Structure of γ-Al2O3 by High-Field Solid-State NMR Spectroscopy. *Nat. Commun.* **2020**, *11* (1), 3620.
(23) Martins, V.; Xu, J.; Wang, X.; Chen, K.; hung, i.; Gan, Z.; Gervais, C.; Bonhomme, C.; Jiang, S.; Zheng, A.; Lucier, B. E. G.; Huang, Y. Higher Magnetic Fields, Finer MOF Structural Information: 17O Solid-State NMR at 35.2 T. *J. Am. Chem. Soc.* **2020**, *142*, 14877−14889.
(24) Gao, W.; Qi, G.; Wang, Q.; Wang, W.; Li, S.; Hung, I.; Gan, Z.; Xu, J.; Deng, F. Dual Active Sites on Molybdenum/ZSM-5 Catalyst for Methane Dehydroaromatization: Insights from Solid-State NMR Spectroscopy. *Angew. Chem., Int. Ed.* **2021**, *60* (19), 10709−10715.
(25) Dorn, R. W.; Heintz, P. M.; Hung, I.; Chen, K.; Oh, J.-S.; Kim, T.-H.; Zhou, L.; Gan, Z.; Huang, W.; Rossini, A. J. Atomic-Level Structure of Mesoporous Hexagonal Boron Nitride Determined by High-Resolution Solid-State Multinuclear Magnetic Resonance Spectroscopy and Density Functional Theory Calculations. *Chem. Mater.* **2022**, *34* (4), 1649−1665.
(26) Mali, G.; Fink, G.; Taulelle, F. Double-Quantum Homonuclear Correlation Magic Angle Sample Spinning Nuclear Magnetic Resonance Spectroscopy of Dipolar-Coupled Quadrupolar Nuclei. *J. Chem. Phys.* **2004**, *120* (6), 2835−2845.
(27) Wang, Q.; Hu, B.; Lafon, O.; Trébosc, J.; Deng, F.; Amoureux, J. P. Double-Quantum Homonuclear NMR Correlation Spectroscopy of Quadrupolar Nuclei Subjected to Magic-Angle Spinning and High Magnetic Field. *J. Magn. Reson.* **2009**, *200* (2), 251−260.
(28) Hwang, S. J.; Fernandez, C.; Amoureux, J. P.; Cho, J.; Martin, S. W.; Pruski, M. Quantitative Study of the Short Range Order in B2O3 and B2S3 by MAS and Two-Dimensional Triple-Quantum MAS 11B NMR. *Solid State Nucl. Magn. Reson.* **1997**, *8* (2), 109−121.
(29) Kroeker, S.; Stebbins, J. F. Three-Coordinated Boron-11 Chemical Shifts in Borates. *Inorg. Chem.* **2001**, *40* (24), 6239−6246.
(30) Hwang, S.-J.; Chen, C.-Y.; Zones, S. I. Boron Sites in Borosilicate Zeolites at Various Stages of Hydration Studied by Solid State NMR Spectroscopy. *J. Phys. Chem. B* **2004**, *108* (48), 18535−18546.
(31) Angel Wong, Y.-T.; Bryce, D. L. Chapter Four - Recent Advances in 11B Solid-State Nuclear Magnetic Resonance Spectroscopy of Crystalline Solids. In *Annu. Rep. NMR Spectrosc.*; Webb, G. A., Ed. Academic Press: 2018; Vol. 93, pp 213−279.
(32) Dorn, R. W.; Ryan, M. J.; Kim, T.-H.; Goh, T. W.; Venkatesh, A.; Heintz, P. M.; Zhou, L.; Huang, W.; Rossini, A. J. Identifying the Molecular Edge Termination of Exfoliated Hexagonal Boron Nitride Nanosheets with Solid-State NMR Spectroscopy and Plane-Wave DFT Calculations. *Chem. Mater.* **2020**, *32* (7), 3109−3121.
(33) Medek, A.; Harwood, J. S.; Frydman, L. Multiple-Quantum Magic-Angle Spinning NMR: A New Method for the Study of Quadrupolar Nuclei in Solids. *J. Am. Chem. Soc.* **1995**, *117* (51), 12779−12787.

https://doi.org/10.1021/jacs.2c08237
J. Am. Chem. Soc. 2022, 144, 18766−18771

(34) Frydman, L.; Harwood, J. S. Isotropic Spectra of Half-Integer Quadrupolar Spins from Bidimensional Magic-Angle Spinning NMR. *J. Am. Chem. Soc.* **1995**, *117* (19), 5367−5368.
(35) Brown, S. P.; Wimperis, S. Two-Dimensional Multiple-Quantum MAS NMR of Quadrupolar Nuclei. Acquisition of the Whole Echo. *J. Magn. Reson.* **1997**, *124* (1), 279−285.
(36) Wong, A.; Howes, A. P.; Parkinson, B.; Anupõld, T.; Samoson, A.; Holland, D.; Dupree, R. High-resolution 17O double-rotation NMR characterization of ring and non-ring oxygen in vitreous B2O3. *Phys. Chem. Chem. Phys.* **2009**, *11* (32), 7061−7068.
(37) Brinkmann, A.; Kentgens, A. P. M. Proton-Selective 17O−H Distance Measurements in Fast Magic-Angle-Spinning Solid-State NMR Spectroscopy for the Determination of Hydrogen Bond Lengths. *J. Am. Chem. Soc.* **2006**, *128* (46), 14758−14759.
(38) Dorn, R. W.; Paterson, A. L.; Hung, I.; Gor'kov, P. L.; Thompson, A. J.; Sadow, A. D.; Gan, Z.; Rossini, A. J. Dipolar Heteronuclear Correlation Solid-State NMR Experiments between Half-Integer Quadrupolar Nuclei: The Case of 11B−17O. *J. Phys. Chem. C* **2022**, *126* (28), 11652−11666.
(39) Iuga, D.; Morais, C.; Gan, Z.; Neuville, D. R.; Cormier, L.; Massiot, D. NMR Heteronuclear Correlation between Quadrupolar Nuclei in Solids. *J. Am. Chem. Soc.* **2005**, *127* (33), 11540−11541.
(40) Xin, S.; Wang, Q.; Xu, J.; Feng, N.; Li, W.; Deng, F. Heteronuclear Correlation Experiments of 23Na-27Al in Rotating Solids. *Solid State Nucl. Magn. Reson.* **2017**, *84*, 103−110.
(41) Zheng, M.; Xin, S.; Wang, Q.; Trébosc, J.; Xu, J.; Qi, G.; Feng, N.; Lafon, O.; Deng, F. Through-Space 11B−27Al Correlation: Influence of the Recoupling Channel. *Magn. Reson. Chem.* **2021**, *59* (9−10), 1062−1076.

https://doi.org/10.1021/jacs.2c08237
J. Am. Chem. Soc. 2022, 144, 18766−18771